J Low Temp Phys (2009) 156: 163–181
DOI 10.1007/s10909-009-9891-1

Elementary Vortex Processes in Thermal Superfluid Turbulence

Demosthenes Kivotides · S. Louise Wilkin

Received: 2 February 2009 / Accepted: 17 May 2009 / Published online: 28 May 2009

Abstract By solving pertinent mathematical models with numerical and computational methods, we analyze the formation of superfluid vorticity structures in a turbulent normal fluid with an inertial range exhibiting Kolmogorov scaling. We demonstrate that mutual friction forcing causes quantum vortex instabilities whose signature is spiral vortical configurations. The spirals expand until they accidentally meet metastable, intense normal fluid vorticity tubes of similar curvature and vorticity orientation that trap them by driving them towards low mutual friction sites where superfluid bundles are formed. The bundle formation sites are located within the tube cores, but, due to tube curvature and many-tube interaction effects, are displaced by variable distances from the tube centerlines as they follow the contours of the latter. We analyze possible implications of these processes in fully developed thermal superfluid turbulence dynamics.

Keywords Thermal superfluid turbulence · Vortex dynamics · Numerical computation

PACS 67.25.dk · 47.32.cb · 47.37.+q

1 Introduction

Thermal superfluids represent a particularly complex case study in nonlinear and statistical physics, since they are characterized by strongly coupled, nonlinear fluctuations over extensive scale ranges. The main challenge in their mathematical study is the construction and analysis of dynamical models of the structure of these fluctuations in specific scale-ranges, and, subsequently, the connection of these models in

D. Kivotides (✉) · S.L. Wilkin
Department of Chemical Engineering, University of California, Santa Barbara, CA 93117, USA
e-mail: demos@engineering.ucsb.edu

order to achieve a conceptually continuous description valid over all scales. In this vein, microscopic models within the framework of quantum field theory have been proposed [1–4], as well as mesoscopic (kinetic regime) models employing a generalized version of the Gross-Pitaevskii equation for the superfluid and a quantum Boltzmann equation for the normal fluid [5, 6]. The fact that the microscopic quantum field theory does not lead, in the quantum fluids case, to the classical Liouville equation and from there to the classical Boltzmann equation (as it does in classical fluids) has to do with both that (a) the wavelength of the wavefunction associated with the constituent molecules is larger than the interparticle distance, and (b) molecule mobility allows, by enabling particle position interchanges, quantum statistics, i.e., of the effects of particle indistinguishability, to be active (in the quantum fluids case) in all pertinent space-time scales [1]. Moreover, superfluids are a special case of quantum fluids since they exhibit the intrinsic phenomenon of Bose-Einstein (^{4}He and alkali gases) or Cooper-pairing (^{3}He and electron liquid in conducting solids) condensation. Without condensation phenomena, the macroscopic behaviour of quantum fluids would have been reduced to the hydrodynamics of the normal fluid component which is not phenomenologically different to classical hydrodynamics. Notwithstanding their generality, the computational complexity of the aforesaid models does not allow the practical computation of large superfluid systems. Hence, macroscopic scale models based on continuum mechanical theory [7–12] in which only the hydrodynamic scales are treated have also been employed. In the latter, both superfluid and normal fluid are depicted as continuous systems, although the discrete nature of superfluid vorticity (in the form of isolated vortex lines) is explicitly taken into account. Finally, at hyper-macroscopic scales even the superfluid vorticity becomes a continuous field [13, 14].

The present contribution focuses on the macroscopic fluid mechanical regime, and in particular on the most general flow state in this realm in which both normal fluid and superfluid velocities fluctuate [15, 16]. Due to their vortical and deterministic nature, these nonlinear fluctuations are classified as turbulent. An intuitive way of understanding the structure of fluctuating systems could involve (if possible) the identification of (at least metastable) structural elements that dominate their complex phenomenology and carry most of the fluctuation energy shaping the fluctuation statistics via their interactions. In athermal superfluids, the quantized line vortices are examples of such structural elements. In thermal superfluids, the addition of the normal fluid complicates the situation, since the reduction of turbulence phenomenology to interactions between a complex system of vortex tubes has only (a vigorously debated) approximate validity [17–20] in the classical Navier-Stokes equation that describe the physics of the normal component. In this context, the vortex tube model (VTM) of Kivotides and Leonard [21, 22], based on a postulated "quantization" of classical (normal fluid) turbulence in terms of linear vortical structures (see also relevant discussions in Refs. [23, 24]), was shown to reproduce basic statistics of inertial range Navier-Stokes turbulence, and has been employed as an intuitive model of large scale velocity field physics in various disciplines [25, 26]. Thus, it appears that a basic understanding of interactions between the aforesaid classical and superfluid vorticity structures could provide significant insight into the fundamental flow processes behind turbulence fluctuations in thermal superfluids. These ideas have inspired the analysis performed in the present contribution.

Previously, Vinen [27] modeled turbulence eddies in both fluids as rigid spheres, and by employing dimensional and scaling analysis, as well as an approximate formula for the mutual friction force, concluded that under certain conditions the large scale dynamics of the two fluids would be identical (fully coupled). This understanding, which is also employed in the analysis of Stalp et al. [15] indicates a much stronger effect than a simple tendency of alignment between the vorticity of the two fluids. Barenghi et al. [28] continued Vinen's approach by considering slightly more complicated flow models and argued for a tendency of alignment of the two vorticities. They heuristically coupled their findings with standard scaling theories of classical turbulence (i.e., ignoring the effects of the superfluid on the structure of normal fluid turbulence) and reached similar conclusions to Vinen's.

These studies indicate important physics, but they (essentially) analyze simple flows not necessarily relevant to complex turbulent flows. Indeed, Barenghi et al. [28, 29] have studied superfluid vorticity dynamics in a kinematic, single scale ABC normal flow and observed a polarization of the quantum vortex tangle by normal fluid vorticity which, in this flow, is organized in a system of straight (nonplanar) vortices. Samuels [30] went a step further, and by calculating the dynamics of quantized vortices under the influence of a kinematic, straight normal fluid vortex tube, suggested an explicit mechanism of superfluid tangle polarization. He has shown that an initial superfluid ring becomes distorted by the normal fluid vortex that pulls the similarly aligned hemicircle towards it and traps it within its core. Subsequently, the Ostermeier-Glaberson instability causes the part of the loop connecting the free, anti-aligned hemicircle with the trapped one to generate a new vortex loop. Samuels showed that subsequent multiple repetition of this process accumulates quantized vortices within the normal vortex core, and conjectured that, at large times, the circulations in the two fluids are matched.

Whilst such studies have offered valuable insights, direct extrapolation of these results to fully developed turbulent normal flow is difficult to justify. First, in normal fluid turbulence there are many, curved, dynamic vortices that generate a multiscale fluctuation field with the Kolmogorov spectrum. Their physics are influenced by the superfluid vortices via mutual friction effects which are absent in kinematic normal fluid descriptions. Equally important, the aforesaid studies have not included both mutual friction terms, and, despite the work of Idowu et al. [31], have not employed the mutual friction force equations that are consistent with a normal flow velocity modeled after the Navier-Stokes equation. Since the Kolmogorov spectrum applies to a local (Navier-Stokes) normal velocity field and not to a spatial average of it obeying HVBK type equations, it is difficult to justify (in the superfluid vortex dynamics equations) mutual friction models that involve HVBK type averages of the normal fluid velocity. Kivotides [32] addressed some of the aforesaid issues by modeling an interaction of superfluid vortices with a snapshot of homogeneous, isotropic normal fluid turbulence that was generated by the VTM model and presented an inertial range with Kolmogorov scaling. The advantage of his approach is that it combines the complexity of Navier-Stokes model turbulence with explicit information about coherent vorticity structure physics. Moreover, the calculations included both mutual friction force components employing their local normal fluid velocity formulation [31].

The analysis has shown that the normal vortex tubes induce superfluid vortex bundles of strength comparable with the normal fluid tubes. These bundles form within

the normal fluid vortex cores but somewhat offset from their centerlines. Bundle formation comes together with the emergence, in the superfluid energy spectrum, of an inertial range with Kolmogorov scaling. We note parenthetically that the computed superfluid bundles could be thought of as discrete, inviscid analogues of normal/classical fluid vortex tubes, so it is not surprising that a similar result (regarding an inertial regime with Kolmogorov scaling) was also obtained by Kivotides and Leonard via VTM [21] in the context of classical turbulence. Kivotides [32] also demonstrated that self-stretching of superfluid bundles of quantized vorticity coincides with a direct energy cascade in wavenumber space (a process also considered to be crucial in classical fluid turbulence physics [17]). Another aspect of his analysis was the description of an inverse vorticity cascade via bundle braiding processes that result in bundle fusion. So the superfluid bundles become thinner by self-stretching (and cascade energy to smaller scales), but become fatter by the aforesaid braiding process. The braiding process is a necessary condition (when for example the external forcing has ceased and there is no new coherent structure formation) for the existence of a (strongly intermittent) energy cascade, since without the bundle fattening (via braiding) process there could be no bundle core stretching process. In other words, the braiding process is a way of allowing the inertial effects to achieve simultaneously (during vortex bundle fusion) these two, seamingly opposite, processes. Indeed as shown in references [32, 33] bundle fusion coincides with strongest vortex stretching. Overall, superfluid turbulence involves the formation by self-organizing mutual friction action of quantized vorticity bundles that grow thicker by braiding while at the same time (for the particular strength of inertial forces in the flow) become thinner by stretching, transporting energy to smaller scales. In this way, most of the cascade physics involves the potential flow outside vortex bundle cores rather than the (approximately) solid body rotation within the latter. This scenario could be compared with an analogous one in the classical case [44], where it is thought that Navier-Stokes dynamics produce first vortex sheets that roll-up via Kelvin-Helmholtz instabilities into fine spiral vortical structures that fuse into classical vortex tubes via viscous action. In the classical case, one needs a large scale forcing (for example, included self-consistently in fluid-structure interaction theories) that would provide the energy needed for the formation of the near singular vortex tubes, and a viscous force to dissipate the cascaded energy. In this context, Kivotides [32, 33] offered quantitative proof that both of these functions in the bundle system are performed by mutual friction (i.e., by the normal fluid).

However, despite these findings, the crucial aspect of an explicit bundle formation mechanism (on par with the analysis of Samuels [30]) is lacking. Equally important, the serious deficiencies of the kinematically prescribed normal fluid, and the lack of any normal fluid dynamics remain. The latter issue was tackled by Morris et al. [34] who employed fully developed Navier-Stokes turbulence in order to generate superfluid turbulence, and found a tendency of alignment between the large scale averages of the two vorticities. There was, however, no explicit information on the formation of superfluid bundles and their trapping by coherent normal vortical structures or their combined subsequent movement as one fully coupled vortical structure as suggested by Vinen [27]. Notwithstanding the sophistication of their computation, Morris et al. did not offer an explicit mechanism for the alignment process, and did not employ the

local normal flow velocity formulation of the mutual friction forces that is consistent with their fully resolved Navier-Stokes turbulence in the normal fluid.

In this contribution, we first analyse Samuels' [30] problem, employing a formulation which included two mutual friction forces [31]. We demonstrate the basic phenomenology of the interaction between superfluid vorticity and a straight normal vortex tube, and, subsequently, we identify elements of this phenomenology on the more complicated problem of the interaction of quantum vortices with a multiscale (although still kinematic) turbulent vortical structure. Note that, in similarity with the VTM calculation of [32, 33], the normal fluid vortices are static by default. By explicitly showing how superfluid vortices are trapped by normal fluid turbulence vorticity structures, we facilitate the interpretation of more powerful fully coupled turbulence calculations that are presently pursued.

2 Mathematical Model and Methods

Both fluids are modeled as vortex dynamical systems. Since in our approach the superfluid vorticity is not continuous but discrete (individual line vortices), we need to use a superfluid vortex dynamics equation that employs the local normal fluid velocity at the quantized vortex positions. It is not consistent to employ an averaged normal fluid velocity that obeys HVBK type of equations, since, at the length scales where the latter formalism is valid, the superfluid vorticity is continuous. Idowu et al. [31] have derived a suitable vortex dynamical equation that we use here. Notably, the latter equation does not simply involve a rescaling of the α and α' mutual friction coefficients in the equation employed in references [30, 39]; it is a different equation. In particular, let $\boldsymbol{X}_s(\xi_s, t)$ denote the superfluid vortex tangle $\mathcal{L}_s$ where ξ_s is the arclength parametrization along the vortex loops, and t is time. The evolution equation for $\boldsymbol{X}_s(\xi_s, t)$ is given by [10]:

$$\frac{\partial \boldsymbol{X}_s}{\partial t} = \boldsymbol{V}_s + h_1 \boldsymbol{X}_s' \times (\boldsymbol{V}_n - \boldsymbol{V}_s) + h_2[\boldsymbol{X}_s' \times (\boldsymbol{X}_s' \times \boldsymbol{V}_n) + \boldsymbol{V}_s], \tag{1}$$

where $\boldsymbol{V}_n$ is the normal fluid velocity and the superfluid velocity $\boldsymbol{V}_s$ is given by the Biot-Savart integral:

$$\boldsymbol{V}_s(\boldsymbol{x}) = -\frac{\kappa}{4\pi} \int_{\mathcal{L}_s} \mathrm{d}\xi_s \frac{\boldsymbol{X}_s' \times (\boldsymbol{X}_s - \boldsymbol{x})}{|\boldsymbol{X}_s - \boldsymbol{x}|^3}. \tag{2}$$

Here, $\boldsymbol{X}_s' \equiv \partial \boldsymbol{X}_s / \partial \xi_s$ is the unit tangent vector (indicating the direction of the singular superfluid vorticity), κ is the quantum of circulation and h_1, h_2 are known dimensionless mutual friction parameters [35].

The computational superfluid vortex model includes topological changes in the tangle geometry via reconnections. Feynman [38] was first to suggest them, and Schwarz [39] was first to introduce them in computational studies. They give rise to the equation

$$\mathcal{T}_{\mathcal{L}_s}(t) \longmapsto \mathcal{T}'_{\mathcal{L}_s}(t), \tag{3}$$

with $\mathcal{T}_{\mathcal{L}_s}(t)$ denoting the topology of $\mathcal{L}_s$ at time t. At each time step, we compute the minimum of grid resolution along the vortices' contours and intervortex distance, and we instantaneously reconnect two vortices when their distance becomes smaller than the a fraction $f_s = 0.1$ of this minimum.

The model for the normal fluid vortices is described in detail in [21, 36] and references therein. The velocity of the normal fluid at field position $\boldsymbol{x}$ is given by the Biot-Savart integral

$$\boldsymbol{V}_n(\boldsymbol{x}) = -\frac{1}{4\pi}\int \frac{(\boldsymbol{x}-\boldsymbol{x}')\times\boldsymbol{\omega}_n(\boldsymbol{x}')\mathrm{d}\boldsymbol{x}'}{|\boldsymbol{x}-\boldsymbol{x}'|^3}, \tag{4}$$

where, notably, the integral is over all space, and the normal fluid vorticity $\boldsymbol{\omega}_n$ is distributed within the normal fluid filament cores [36]

$$\boldsymbol{\omega}_n(\boldsymbol{x},t) = \sum_i \Gamma \int_{C_i} \frac{1}{\sigma_i(\xi_n,t)^3}\zeta\left(\frac{|\boldsymbol{x}-\boldsymbol{X}_n^i(\xi_n,t)|}{\sigma_i(\xi_n,t)}\right) \times\left(\frac{\partial \boldsymbol{X}_n^i}{\partial\xi_n}+\frac{\boldsymbol{x}-\boldsymbol{X}_n^i(\xi_n,t)}{\sigma_i(\xi_n,t)}\frac{\partial\sigma_i}{\partial\xi_n}\right)\mathrm{d}\xi_n. \tag{5}$$

Here, C_i is the centerline contour of filament i, ξ_n is the arclength parametrization, and $\sigma_i(\xi_n)$ is the core radius along the same filament. The smoothing kernel ζ describes the way vorticity spreads around the core centerline. The calculations are done with the Gaussian kernel of [37]

$$\zeta_g\left(\frac{r}{\sigma}\right) = \frac{1}{(2\pi)^{\frac{3}{2}}}e^{-r^2/(2\sigma^2)}. \tag{6}$$

Moreover, Γ is the circulation strength attributed by the VTM "quantization" to all filaments, and is the VTM model's analog of the quantum of circulation. It is related to the Reynolds number by $\mathrm{Re} = \Gamma/\nu_n$, where ν_n is the kinematic viscosity of the normal fluid. Inserting the above definition of vorticity in the Biot-Savart integral reduces the latter to a sum of line integrals over each filament centerline contour

$$\boldsymbol{V}_n(\boldsymbol{x}) = -\frac{\Gamma}{4\pi}\int_{\mathcal{L}_n}\mathrm{d}\xi_n\frac{Q(\phi)}{(\sigma(\boldsymbol{X}_n)^2+\sigma(\boldsymbol{x})^2)^{3/2}}\boldsymbol{X}_n'\times(\boldsymbol{X}_n-\boldsymbol{x}), \tag{7}$$

where $\mathcal{L}_n$ denotes the normal vortex centerline tangle and function $Q(\phi)$ (with $\phi = |\boldsymbol{X}_n-\boldsymbol{x}|/(\sigma(\boldsymbol{X}_n)^2+\sigma(\boldsymbol{x})^2)^{1/2}$) depends on the particular smoothing kernel ζ_g employed [37, 42]. For the Gaussian kernel case, it is

$$Q(\phi) = \frac{\mathrm{erf}(\phi/\sqrt{2})-\sqrt{\frac{2}{\pi}}\phi e^{-\phi^2/2}}{\phi^3}, \quad \boldsymbol{X}_n\neq\boldsymbol{x}, \tag{8}$$

$$Q(\phi) = \sqrt{\frac{2}{9\pi}}, \quad \boldsymbol{X}_n = \boldsymbol{x}. \tag{9}$$

Notably, this desingularization of the Biot-Savart kernel gives zero self-induced velocity for a differential element. In this way, its velocity is determined by the neighbouring elements. As in athermal superfluids, the normal filament centerlines move with the local normal fluid velocity

$$\frac{\partial \boldsymbol{X}_n}{\partial t} = \boldsymbol{V}_n. \tag{10}$$

Notably, according to Leonard's model (5) there can not be helical vortex lines around the vortex-core center lines, and therefore axial flow inside the cores. It is important to note that in normal fluids vortex contour dynamics alone does not capture all physics. One needs a way of updating the tube radii. Biot-Savart motion changes vortex length, and this in turn results in tube radii dynamics according to the law of filament volume conservation during inviscid evolution

$$\frac{\mathrm{d}}{\mathrm{d}t}\left(\sigma(\boldsymbol{X}_n)\left|\frac{\partial \boldsymbol{X}_n}{\partial \xi_n}\right|\mathrm{d}\xi_n\right) = 0, \tag{11}$$

which is applied to each discrete vortex segment at each time step, and it is a direct consequence of the incompressibility of the fluid and the fact that in Euler dynamics vortex lines move with the fluid velocity. The combination of this law with the solenoidal character of the vorticity field is responsible for the intriguing phenomenon of enstrophy intensification in classical turbulence dynamics via vortex stretching. Although this vortex stretching effect is absent from superfluid line vortex dynamics, it is active in superfluid vortex bundle dynamics, and its physical consequences in thermal superfluid turbulence context are discussed in references [10, 21, 32]. In addition, normal fluid vortex cores are growing due to the diffusive part of molecular fluctuations (which do not preserve filament volume). This effect is captured with the core spreading method [43]

$$\frac{\mathrm{d}\sigma^2}{\mathrm{d}t} = 2\gamma\nu_n, \tag{12}$$

where γ is a factor depending on the particular kernel ζ_g employed, and is equal to $\gamma = 1$ for our Gaussian choice of kernel.

Similarly with the superfluid case, normal fluid vortices reconnect. Vortex reconnection in classical fluid dynamics is a standard, intensively studied topic. A computational approach to classical filament reconnection in a vortex-dynamical context was developed by Kivotides and Leonard [40]. The corresponding equation is

$$\mathcal{T}_{\mathcal{L}_n}(t) \longmapsto \mathcal{T}'_{\mathcal{L}_n}(t), \tag{13}$$

with $\mathcal{T}_{\mathcal{L}_n}(t)$ denoting the topology of $\mathcal{L}_n$ at time t. We instantaneously reconnect two vortices when their distance becomes smaller than a fraction $f_n = 0.5$ of the sum of their local tube radii. Note that filament volume is not conserved during reconnections since the latter rely on the relative slip of the vorticity field with respect to the fluid (i.e., they do not move with the material velocity) as this is effected by viscous action, and so the tube volume can change. In our computational model, we keep the tube radius of the reconnecting filament during reconnection constant, and we adjust the

reconnecting differential element volume taking into account the post-reconnection topology.

The above set of equations was solved with numerical methods that have been extensively discussed in the cited references. Although, in all cases presented here, the superfluid vortices interact with stationary normal vortices, classical filament dynamics are needed to achieve the homogeneous, isotropic turbulence state employed in the study of interactions between quantized vortices and turbulence.

3 Results

Since we intend to understand the structure and energetics of homogeneous thermal superfluid turbulence, we impose in all computations periodic boundary conditions. The working superfluid is ^{4}He; similar mathematical models are also applicable to ^{3}He-B, although the typical phenomenology of ^{3}He-B flows is expected to differ from the ^{4}He case since the material properties that enter as parameters in these equations differ significantly between the two fluids [8, 41]. We fix the temperature at $T = 1.3$ K so that $\nu_n = 2.3303 \times 10^{-3}$ cm^2/s, $h_1 = 0.04093$, and $h_2 = -0.02175$. Notably, the two mutual friction coefficients are of the same order and opposite sign. Since the magnitude of the second coefficient is approximately half of the first, its effects can not be neglected. When two superfluid vortices reach a certain close proximity (specified below) they reconnect. We have verified that our results do not depend on this cut-off distance.

3.1 Straight Normal Fluid Vortex

The size of the computational box is $l_b = 0.005$ cm. Within it, we place a straight normal fluid vortex tube and a seed superfluid vorticity in the form of a vortex ring. The straight normal fluid vortex circulation corresponds to $\mathrm{Re} = 400$. This gives $\Gamma/\kappa = 934.92$, thus inertial effects in the normal fluid grossly overpower corresponding effects in the superfluid, and the effects of mutual friction on the quantized vortices are dominant. The vortex tube radius is chosen to be $\sigma = 0.1\ l_b$. Note that, according to the definition of the employed Gaussian smoothing kernel, σ does not imply a sharp cut-off of normal vortex tube vorticity at this distance; it only delineates the region of highest vorticity. In order to ensure a smooth normal fluid velocity field, we densely discretize the normal vortex contour: the size of the vortex segments is $\delta l_n = 0.1\sigma$. The superfluid vortices are discretized in segments of length $\delta l_s = l_b/32$. The reconnection cut-off is set to $0.1\ \delta l_s$. The numerical time step that resolves all Kelvin waves present in the system is $\delta t = 6.9 \times 10^{-6}$ s. The size of the quantized vortex ring is of the order of the system size; its diameter is $D = 0.2 l_b$. We have experimented with various ring orientations and positions within or outside the tube core. For sufficiently strong normal circulation strengths, they all gave similar results. In order to ensure that the quantized ring will interact rapidly with the normal vortex tube, we have placed the ring in a collision course with the tube at distance equal to $0.25D$. Moreover, normal vortex circulation and system size give, for the characteristic time scale $\tau = l_b^2/\Gamma$, the value $\tau = 2.68 \times 10^{-5}$ s. We calculate at least

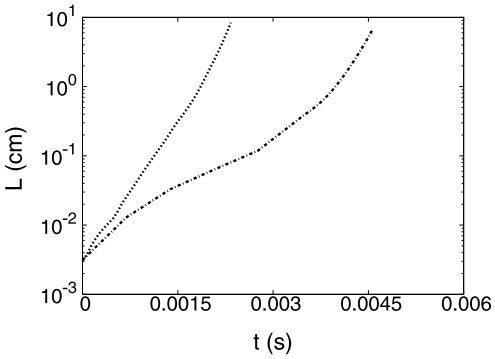

Fig. 1 Superfluid vortex length (cm) vs time (s) when (a) the local normal fluid velocity is employed and both mutual friction components are taken into account (fast growing *dashed line*), and (b) the average normal fluid velocity is employed and only one mutual friction component is taken into account as in [30] (*dot-dashed line*). At large times, both computations show exponential increase

two orders of magnitude beyond this time in order to ensure that all transients have ceased. Finally, we have also made a complementary computation using the equations employed in [30] in order to compare the two solutions.

The evolution of the superfluid vortex length is shown in Fig. 1. As expected, the formulation employing both mutual friction coefficients results in enhanced energy transfer from the tube to the superfluid. In agreement with Samuels [30], we also find that the Ostermeier-Glaberson instability generates new loops and a portion of them becomes trapped by the vortex core. Only vortices that find themselves in the neighbourhood of the vortex centerline (i.e., within the intense vorticity region) and (at the same time) extend approximately along the vortex direction are trapped. Certain dynamical processes limit the strength of the trapping mechanism. In particular, the first (i.e., associated with h_1) mutual friction force component causes loops on planes normal to the vorticity tube to become three-dimensional facilitating vortex reconnections with other similarly affected loops. These reconnections have in general a disorganizing effect. On the other hand, the second (i.e., associated with h_2) mutual friction force component tends to blow up such loops creating planar-like outward-spiraling vortex configurations (that escape the influence of the core). These are depicted in Fig. 2 which shows the projection of line vortex geometry on the plane normal to the tube.

In the context of these findings, we mention that fully resolved Navier-Stokes computations [44] show that small scale classical (normal fluid) turbulence structure is characterized by straight, stretched vortices. Burgers vortices, for which dissipation is counterbalanced by a uniform straining field, are examples of such structures. Thus, assuming that our straight tube (which, like the Burgers vortex, has a constant core radius) is representative of small scale normal vorticity structure, the computed spiral structure could be relevant to the high-frequency behaviour of quantized vorticity in recent thermal superfluid turbulence experiments [45, 46], i.e., measured spectra could correspond (at high wavenumbers) to the spectra of quantum vortex spirals. Their energy spectrum (computed as discussed in [10]) is displayed in Fig. 3, and shows a low wavenumber scaling of k^{-3} which is reminiscent of the scaling of two dimensional classical turbulence in the large scale, direct enstrophy cascade regime. Similarly, since the quantum vortex spirals extend on planes normal to the straight tube, one expects a poor correlation between the two fluid vorticities at small scales in fully developed (kinematic normal fluid) thermal superfluid turbulence. This could

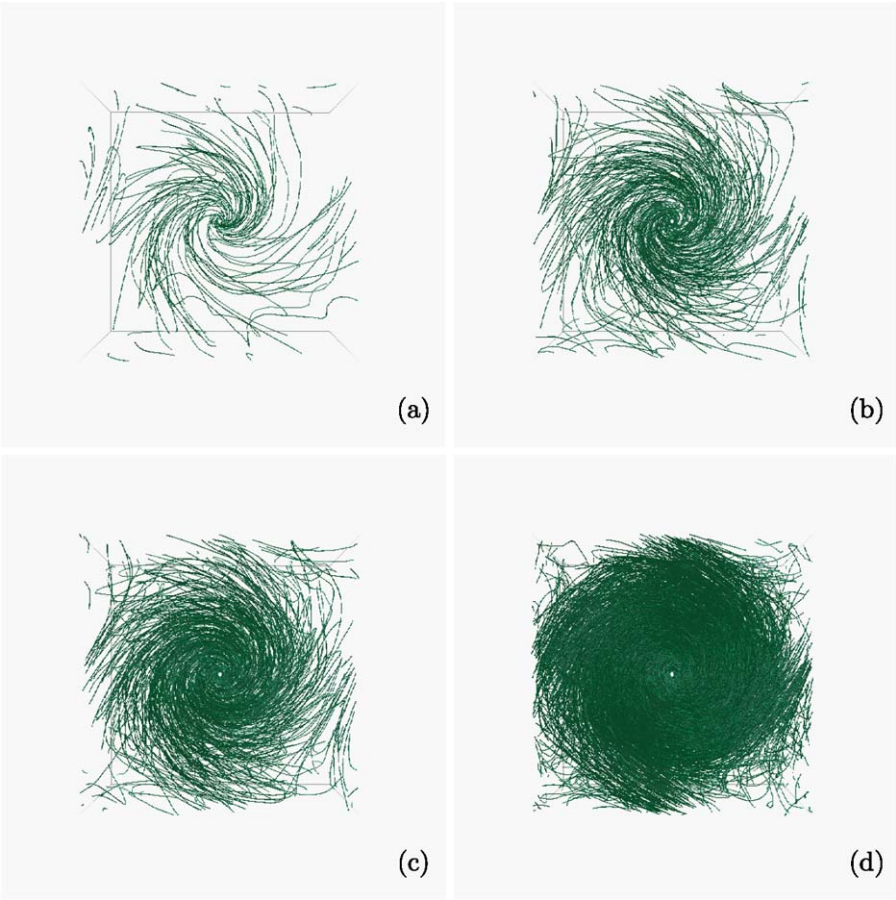

Fig. 2 (Color online) Projection of superfluid vortex centerline geometry on a plane normal to the normal fluid tube. The vorticity tube is shown with one tenth of its full radius, and appears as a central *white dot*. The formation of outward-spiraling vortices is the dominant dynamical effect. The corresponding graph times are: $t_a = 1.588 \times 10^{-3}$ s, $t_b = 1.912 \times 10^{-3}$ s, $t_c = 2.050 \times 10^{-3}$ s, $t_d = 2.339 \times 10^{-3}$ s

Fig. 3 Energy spectrum of the spiral structure shown in Fig. 2 (largest time). A k^{-3} fit at low wavenumbers is also shown. Note that the wavenumbers are defined without the 2π factor, i.e., $k = 1/\ell$ where ℓ has units of length

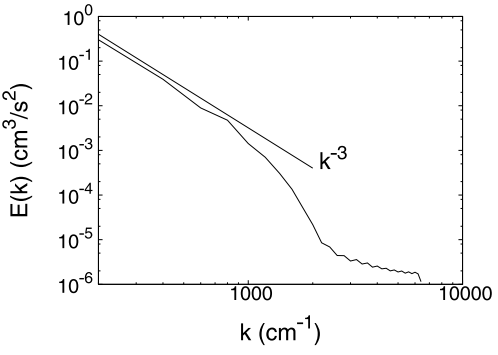

explain the similar finding of Ref. [34]. Finally, sufficiently perturbed axisymmetric vortices [47] lead to classical spiral vortices that are also employed as models of the finest turbulence structure [48]. There is a notable similarity between the computed quantized vorticity spiral and spiraling patterns of passive scalar dispersion by these classical spiral vortices [48, 49]. Notably, at final time, the superfluid tangle is so dense that the kinematic description of the normal fluid is not appropriate. The model applies only to appropriately dilute quantum vortex tangles, and long time results are merely shown in order to demonstrate that all transients have ceased, and that we have indeed achieved a steady state (in terms of tangle organization since the vortex length keeps increasing at this time).

How important is the effect calculated by Samuels in Ref. [30]? The graphs of Fig. 4, show the way superfluid vorticity builds up within the normal tube for the

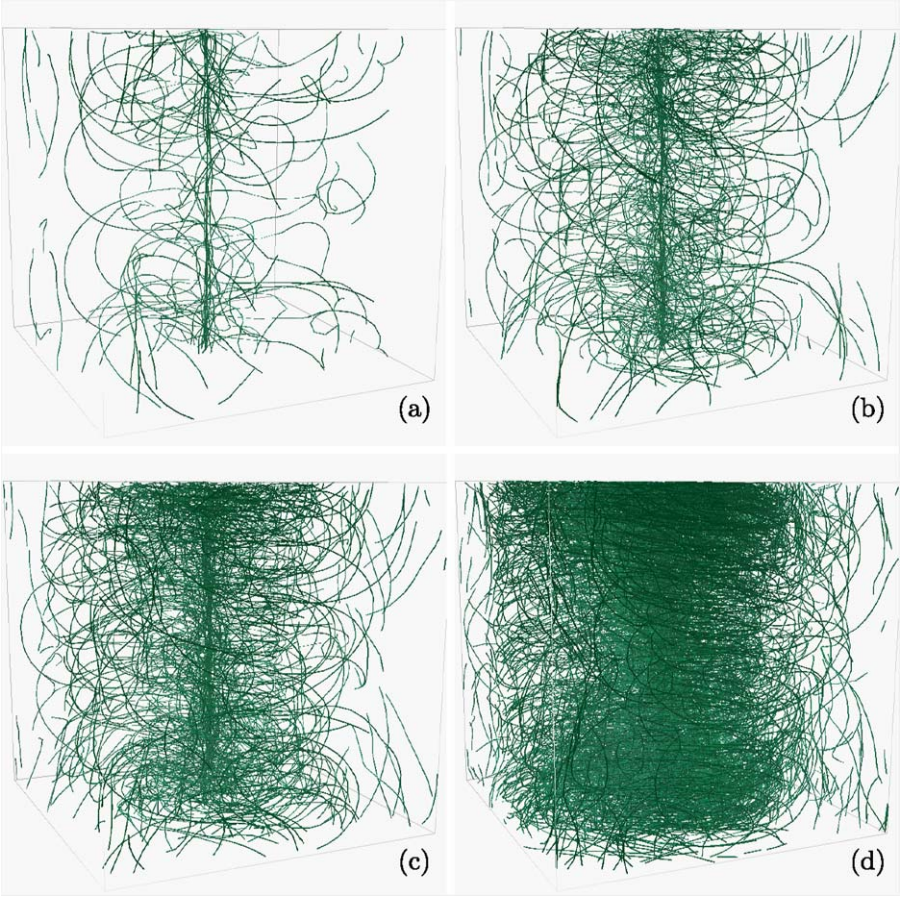

Fig. 4 (Color online) The formation of a superfluid bundle within the core of the (not shown) normal vortex tube. At the final time, the circulation of the induced bundle is much smaller than (less than 5% of) the circulation of the normal tube. The corresponding graph times are: $t_a = 1.588 \times 10^{-3}$ s, $t_b = 1.912 \times 10^{-3}$ s, $t_c = 2.050 \times 10^{-3}$ s, $t_d = 2.339 \times 10^{-3}$ s

same times as in Fig. 2. At the final time, we can count a few dozen (not more that 50) superfluid vortices comprising a bundle that coincides with the normal fluid tube. Noting that the normal circulation is approximately 1000κ, the results do not support the formation of a superfluid bundle of strength equal to the normal tube. Similar conclusions were allowed by the results of the computation neglecting the second (i.e., h_2) mutual friction coefficient. Noting that the total quantum vortex length at the final time is 8.3849 cm, and that the total length involved in the bundle is (at most) approximately 0.25 cm, only a small fraction of the total length is obviously organized within the tube core. Certainly, the less organized part could also tend to align with the tube axis and so to couple the two fluids. However, while trying to understand the structure of thermal superfluid turbulence, one can not neglect the majority of the superfluid vorticity induced, especially since it appears to be much more structured in the form of the aforesaid spiral. Next, we shall show that in the more complicated case of a turbulent normal fluid tube system, the formation of large scale bundles relies on the ability of intense normal fluid vorticity to trap superfluid vortices of similar geometry and vorticity direction. However, due to the curvature of realistic [21] large scale normal tubes, the Samuels mechanism of bundle formation is not active; instead, the bundles are formed when normal tubes capture the aforesaid outward-spiraling quantum vortices originating in Obermeier-Glaberson instability processes that took place in the vicinity of other normal tubes. Thus, in general, the superfluid vortices are trapped by a different intense vorticity region than the one that created them at the first place.

3.2 Turbulent Normal Fluid Vortex Tangle

In Ref. [32], Kivotides has shown that in a model, structured turbulent flow, with many curved normal fluid tubes and an inertial range exhibiting Kolmogorov scaling, superfluid vortex bundles (bound states of quantized vorticity) form in between the normal vortex centerlines (but within their cores). The bundles gain strength until they acquire their own independent dynamics when their circulation is approximately 10% of the normal tube circulation. Subsequently, they interact strongly with each other, and by fusing via braiding they gain strength until their circulation becomes comparable with the circulation of the normal tubes [32]. Although this "independence" threshold is an artifact of the lack of dynamical effects in the kinematic description of the normal fluid, the post-escape physics of superfluid bundles described in [32] could be an informed approximation to the kinematics of quantized vorticity in fully developed thermal superfluid turbulence. Here, we perform a similar computation with emphasis on the initial stage of coherent structure formation. We indicate connections with the straight tube case, and suggest a structure formation mechanism.

The calculations are done for same conditions as in the straight vortex case, i.e., the working fluid is helium II and $T = 1.3$ K. The normal fluid Reynolds number $\mathrm{Re}_\gamma = \gamma/\nu_n$ (where $\gamma = 932.12 \times 10^{-4}$ cm^2/s is the circulation of the normal fluid vortices) is $\mathrm{Re}_\gamma = 40$. One notes that since $\gamma/\kappa = 93.492$, one normal fluid vortex is as strong as approximately 100 aligned superfluid vortices put together. Similarly to Ref. [32], we first choose a cubic computational domain of size $l_b = 0.1$ cm. Then, we place in it a number of normal vortex loops set at random locations and orientations

Fig. 5 (Color online) The signature of interaction between intense normal fluid vorticity and quantum vortices in a turbulent velocity field is instability generated spiral-like structures. *Left*: superfluid vortices together with normal fluid vortices at time $t = 1.417 \times 10^{-3}$ s. For clarity, the vorticity tubes are shown with 0.08 of their actual core radius σ. *Right*: only the superfluid tangle is shown

with circulation γ defined above. As the loops evolve, they undergo a large number of reconnections, quickly forming a time-dependent turbulent tangle. By checking the statistics of the vortex system, we determine when a statistically isotropic and homogeneous turbulence state with the appropriate Kolmogorov statistics is achieved [21]. We then keep this normal turbulent flow constant in time while we investigate its effect, via mutual friction, on a single initial superfluid vortex ring.

As expected, a sequence of instabilities ensues, and their respective sites emanate quantum vortex spirals as shown in Fig. 5. The arms of these spirals keep expanding, decreasing their curvature until they accidentally (due to the random nature of turbulent normal fluid vorticity) find a normal tube of identical orientation and similar curvature. As discussed above, these two conditions are necessary for the trapping of a quantum vortex by normal vorticity tubes. As the first vortex of a spiral structure slows down under the influence of a normal tube, subsequent arms catch up with it, and their accumulation leads to bundle formation. The various stages of this process, as well as the orientation of normal and superfluid vorticity are shown in Fig. 6. The bundles escape their formation sites once their circulation becomes approximately 10% of the normal vortex circulation. Thus the correlation between their formation sites and their own position is subsequently lost. In a fully consistent computation though, this need not be the case since, as depicted in Fig. 6, a bundle and the normal tube that traps it have similar vorticity orientations and geometry, thus will tend to move in the same direction. Notably, the bundle of Fig. 6 has already formed at $t = 1.719 \times 10^{-3}$ s, that is, two orders of magnitude smaller than the inertial time of the large scale normal turbulent flow, $\tau = l_b^2/\Gamma$ ($\tau = 1.072 \times 10^{-1}$ s). Certainly, this relation between bundle formation time and normal large eddy turnover time does not apply directly to a fully coupled, dynamic Navier-Stokes computation, but it informs that trapping interactions between tubes and quantized vortices are effective in much smaller time than the time needed by a tube of curvature similar to the system size

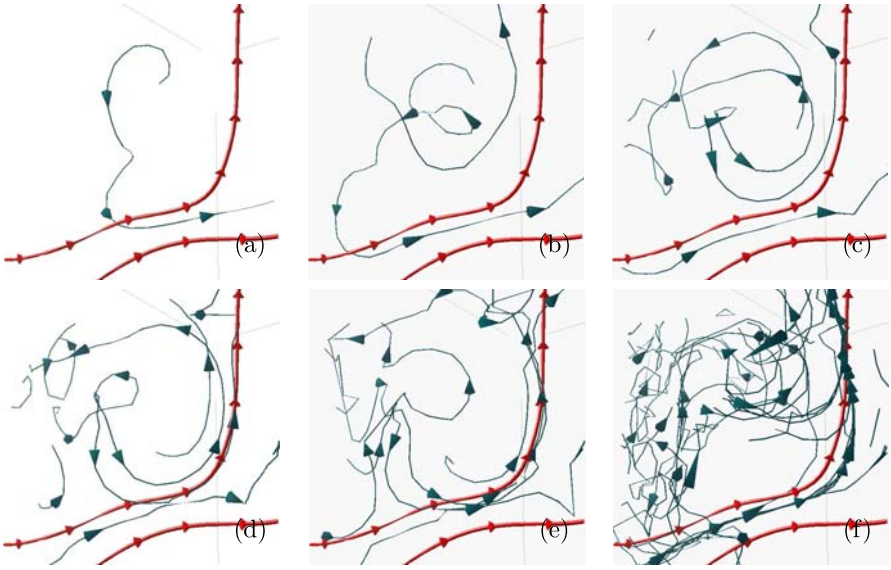

Fig. 6 (Color online) Mechanism of bundle formation in Vortex Tube Model turbulence. The normal tubes (thick, *stationary lines*) are shown with 0.08 of their actual core radius σ. One observes in (**a**) that the first arm of a spiral has approached a normal tube of similar orientation and curvature. In (**b**), the aforesaid vortex is trapped by the normal tube, as subsequent spiral vortices grow due to mutual friction in a similar fashion to the straight normal tube results. As the new spiral arms approach the normal tube (**c**), they slow down under its influence (**d**), and start accumulating (**e**) and eventually form a bundle of six line vortices (**f**). The corresponding times are $t_a = 0.351 \times 10^{-3}$ s, $t_b = 0.646 \times 10^{-3}$ s, $t_c = 0.787 \times 10^{-3}$ s, $t_d = 0.894 \times 10^{-3}$ s, $t_e = 1.013 \times 10^{-3}$ s, $t_f = 1.719 \times 10^{-3}$ s

to transverse the system. Thus, although bundle formation in fully developed superfluid turbulence remains hypothetical at this stage, it appears plausible. According to these results, in a computation based on the more powerfull Navier-Stokes model, the controlling factor of bundle formation would not be so much the dynamic nature of normal fluid vortical structures, but the intensity and duration of their coherence, as well as their geometry. In fully developed superfluid turbulence, the latter are expected to be affected by the back reaction from the bundles on the normal fluid that becomes important some time after the initiation of bundle formation [10].

Notably, as found in Ref. [32], the position of bundle formation does not coincide with the tube centerlines. For example, Fig. 7 shows a bundle formed at distances between 25 and 50 percent of the tube core radius from the centerline. The greater distance between bundle formation site and tube centerline in the low part of the graph has to do with the presence of a neighbouring normal tube (shown in Fig. 6). In fact, the bundle sits just outside the core of this second tube.

Why are bundles offset from the centerlines? In the straight tube case, the quantum vortices are attracted by mutual friction to the center, and stay there since both their self-induction velocity and the normal velocity are zero (solid-body rotation of the core). In turbulence, typical induced bundles shown in Fig. 6, are curved and so posses a self-induced velocity. In order for them to accumulate, this velocity must be approximately counterbalanced by mutual friction effects at the accumulation site.

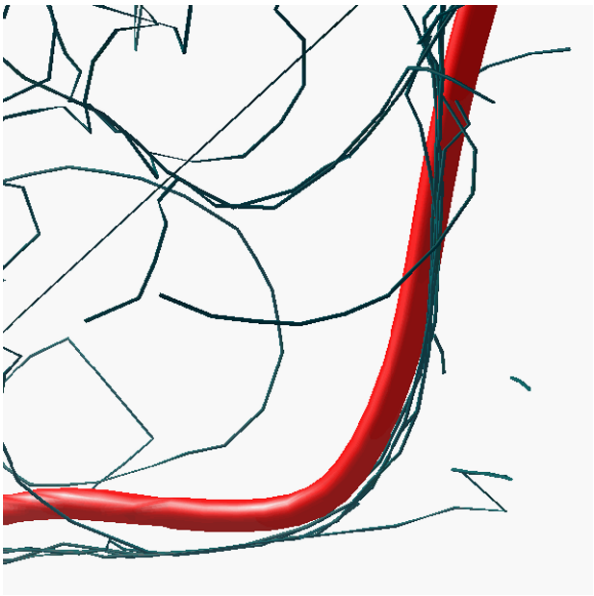

Fig. 7 (Color online) The superfluid bundle formation site follows the outline of the neighbouring, similarly oriented, normal tube of Fig. 6 from a variable displacement. The normal tube is shown with 25% of its actual core diameter, and the bundle sits exactly outside this distance for a significant portion of its contour. The lower bundle part is located at a distance 50% of the tube core from the centerline

Now, the normal fluid velocity field is a complex function incorporating many-tube effects and it is highly unlikely that this cancellation can happen exactly on the tube core centerline. What then determines the distance of the formation sites from the centerlines? Since mutual friction involves the highly energetic normal fluid velocity, and the self-induced superfluid velocity is relatively small, it could be that the bundles' sites coincide with the superfluid tangle positions of small normal fluid velocity (so that mutual friction effects are minimized). Indeed, Fig. 8 demonstrates such a correlation. In particular, at time $t = 1.254 \times 10^{-3}$ s, the maximum normal fluid velocity magnitude along the tangle is $V_n^{mx} = 1798.709$ cm/s, the minimum is $V_n^{mn} = 19.45271$ cm/s, and the average value is $V_n^a = 745.1873$ cm/s. We have then superposed the tangle contour (lines) with the tangle-points (dots) with normal fluid velocity magnitude less than $0.5\ V_n^a$. Only 0.18 of the total number of tangle points satisfy this criterion. As Fig. 8 indicates, they correlate very well with bundle forming sites.

4 Conclusion

4.1 Synopsis

Adding to a series of previous investigations of thermal superfluid turbulence physics, we have demonstrated particular mechanisms of interactions between superfluid vortices and intense normal fluid vorticity. As a rule, normal vortical structures tend to organize quantized vorticity. In the simple case of a straight normal fluid vorticity tube, a dominant organization of the superfluid tangle in the form of a dense spiral was demonstrated. A smaller effect of superfluid bundle formation within the tube

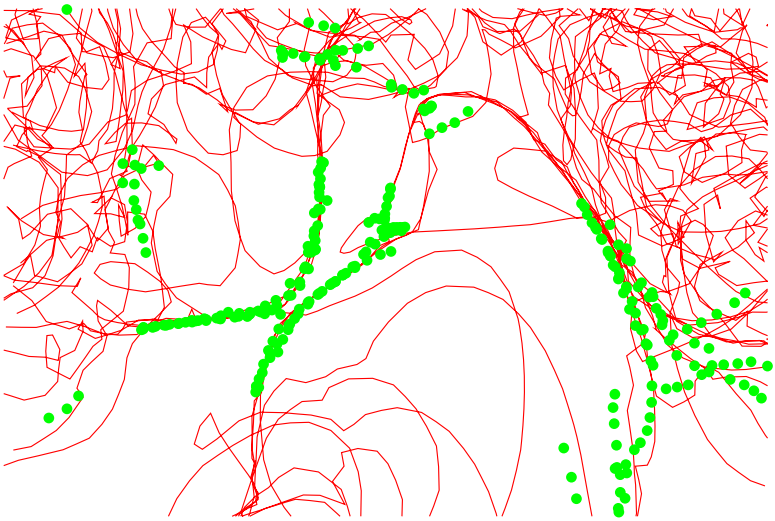

Fig. 8 (Color online) Superposition of tangle contour (*lines*) and tangle points with normal fluid velocity less than half of its average value (*dots*) along the tangle at time $t = 1.254 \times 10^{-3}$ s. The *dots* delineate bundle formation sites to a very good approximation. Note the consistently *undotted large areas* with disorganized superfluid vorticity. Moreover, also consistently, the undotted part of the upper-right bundle has some small residual motion at this time

core (first computed by Samuels in reference [30]) was also indicated. In the complex case of the many, curved tube problem ("VTM turbulence"), tube curvature and many-body effects do not favour the collapse of superfluid loops onto the centerline of the normal tube that caused them to become unstable, and the aforesaid spiral formations are the dynamically important processes. As they expand within a complex net of normal vorticity tubes, they are accidentally arrested by suitable normal fluid tubes with similar curvature and vortical orientation. They are driven to areas of small normal fluid velocity in which the minimized effects of mutual friction counterbalance the self-induced spiral-arms' velocities. Thus, there follows quantum vortex accumulation and bundle formation. Due to tube curvature and many body effects, the bundle formation sites are displaced from the tube centerline positions while still remaining within their cores.

4.2 Outlook

The practice of superfluid computations with kinematic (incompressible) normal fluid is now well developed. From the uniform counterflow velocity profiles employed by Schwarz, to the straight Gaussian vorticity tube of Samuels [30], the ABC flow of Barenghi et al. [28, 29], the fluctuating random harmonic wave flow of Kivotides et al. [50–53], and finally to turbulence via the VTM model computation of Kivotides [32] and the Navier-Stokes model computation of Morris et al. [34]. Although many more studies are needed for a deeper understanding and independent verification of the available results, the latter apply only when the back-reaction of the superfluid on the normal fluid can be neglected. This can be true during the initial stages

of interaction between a seed superfluid vorticity and a highly energetic normal flow, but as the superfluid gains more energy from the normal fluid its back-reaction can not be neglected.

In the past, there have been a number of fully coupled thermal superfluid computations. In particular, Kivotides et al. [9], and Idowu et al. [54] have computed the dynamics of a superfluid ring propagating in an (initially) stationary normal fluid. They found that, in contradistinction to the present study, organized superfluid vorticity induces normal fluid vorticity structures in the form of twin, highly viscous vortices adjacent to the superfluid ring. Subsequently, Kivotides et al. [55] demonstrated that superfluid reconnections enhance the normal fluid dissipation rate thus they augment effective viscosity values. These studies involved relatively simple superfluid vorticity configurations. A step towards higher complexity was undertaken by Kivotides [56] who showed that a turbulent superfluid tangle induces non-inertial vortical fluctuations in an (initially) stationary normal fluid. These fluctuations could be detected with current particle tracking experimental methods and are particularly relevant to a recent experiment of Paoletti et al. [57]. Moreover, since in every normal fluid turbulent flow there are viscosity dominated (low inertia) scales at the high-frequency end of the spectrum, these fluctuations relate to the small scale dynamics of thermal superfluid turbulence and guide the choice of appropriate grid resolutions in inertial turbulence computations as discussed in reference [10]. The latter paper took a further step towards increasing complexity by having the initial superfluid vorticity structured in bundles. As a result, the induced normal fluid turbulence presented fluctuations with a definite inertial range of similar scaling to the Kolmogorov spectrum. Kivotides concluded that superfluid bundles need continuous transfer of energy from the normal fluid in order to be sustained, otherwise they disintegrate. It is important to note that the sudden demise of the superfluid bundles leads to enlarged superfluid vortex line density since the system progresses (during a small time period in comparison with the energy decay rate) from an organized to a disorganized state with essentially similar energies. This sudden increase in vortex line density causes a hump in the graph showing the evolution of superfluid vortex length versus time. Notably, similar humps were observed in the decay of superfluid vorticity by Stalp et al. [15]. These humps could simply be the signature of bundles in the turbulent flow of reference [15] that disintegrate at late stages of normal turbulence decay when (in accordance with [10]) the normal fluid does not have the energy to support its own vorticity structures as well as the superfluid organization (i.e., to keep the entropy of the quantum vortex tangle configuration low). Equally important, these humps were absent in the quantum turbulence decay computation of Kivotides [53] where an unstructured vortical fluctuations field was employed for the normal fluid.

What is needed presently is a collaboration between mathematical theory and experiment that would improve upon the previous indirect argument and offer direct evidence of structures and dynamics. From the experimental side, as discussed by Kivotides and Wilkin [58] the particle tracking method (with its vital capability of following individual particle trajectories) could search for signs of particle-bundle collisions, and computational studies could compute fully coupled thermal superfluid turbulence. Due to their combination of two different fluid dynamical formalisms (i.e., the velocity space description for the normal fluid and the vortex dynamics de-

scription for the superfluid), as well as their resolution requirements, such computations are computationally demanding, and we shall report their findings in a future communication.

References

1. A.J. Leggett, *Quantum Liquids* (Oxford University Press, Oxford, 2006)
2. L. Pitaevskii, S. Stringari, *Bose-Einstein Condensation* (Oxford University Press, Oxford, 2003)
3. M. Mine, M. Okumura, T. Sunaga, Y. Yamanaka, J. Low Temp. Phys. **148**, 331 (2007)
4. M. Kobayashi, M. Tsubota, Phys. Rev. Lett. **97**, 145301 (2006)
5. E. Zaremba, T. Nikuni, A. Griffin, J. Low Temp. Phys. **116**, 277 (1999)
6. B. Jackson, C.F. Barenghi, N.P. Proukakis, J. Low Temp. Phys. **148**, 387 (2007)
7. C.F. Barenghi, R.J. Donnelly, W.F. Vinen (eds.), *Quantized Vortex Dynamics and Superfluid Turbulence* (Springer, Berlin, 2001)
8. A.P. Finne, V.B. Eltsov, R. Hanninen, N.B. Kopnin, J. Kopu, M. Krusius, M. Tsubota, G.E. Volovik, Rep. Prog. Phys. **69**, 3157 (2006)
9. D. Kivotides, C.F. Barenghi, D.C. Samuels, Science **290**, 777 (2000)
10. D. Kivotides, Phys. Rev. B **76**, 054503 (2007)
11. S. Nemirovskii, Phys. Rev. Lett. **96**, 015301 (2006)
12. V.S. L'vov, S.V. Nazarenko, O. Rudenko, Phys. Rev. B **76**, 024520 (2007)
13. H.E. Hall, W.F. Vinen, Proc. R. Soc. Lond. A **238**, 204 (1956)
14. I.L. Bekharevich, I.M. Khalatnikov, J. Exp. Theor. Phys. **13**, 643 (1961)
15. S.R. Stalp, L. Skrbek, R.J. Donnelly, Phys. Rev. Lett. **82**, 4831 (1999)
16. J. Maurer, P. Tabeling, EPL **43**, 29 (1998)
17. P.A. Davidson, *Turbulence* (Oxford University Press, Oxford, 2004)
18. A. Tsinober, *An Informal Introduction to Turbulence* (Springer, Berlin, 2001)
19. M. Farge, G. Pellegrino, K. Schneider, Phys. Rev. Lett. **87**, 054501 (2001)
20. G.L. Eyink, Physica D **207**, 91 (2005)
21. D. Kivotides, A. Leonard, Phys. Rev. Lett. **90**, 234503 (2003)
22. D. Kivotides, A. Leonard, EPL **66**, 69 (2004)
23. G.A. Goldin, R. Menikoff, D.H. Sharp, Phys. Rev. Lett. **58**, 2162 (1987)
24. S.Y. Shishkov, Phys. Lett. A **137**, 272 (1989)
25. D. Kivotides, A.J. Mee, C.F. Barenghi, New J. Phys. **9**, 291 (2007)
26. D. Kivotides, C.F. Barenghi, A.J. Mee, Y.A. Sergeev, Phys. Rev. Lett. **99**, 074501 (2007)
27. W.F. Vinen, Phys. Rev. B **61**, 1410 (2000)
28. C.F. Barenghi, S. Hulton, D.C. Samuels, Phys. Rev. Lett. **89**, 275301 (2002)
29. C.F. Barenghi, D.C. Samuels, G.H. Bauer, R.J. Donnelly, Phys. Fluids **9**, 2631 (1997)
30. D.C. Samuels, Phys. Rev. B **47**, 1107 (1993)
31. O.C. Idowu, D. Kivotides, C.F. Barenghi, D.C. Samuels, J. Low Temp. Phys. **120**, 269 (2000)
32. D. Kivotides, Phys. Rev. Lett. **96**, 175301 (2006)
33. D. Kivotides, J. Low Temp. Phys. **148**, 287 (2007)
34. K. Morris, J. Koplik, D.W.I. Rouson, Phys. Rev. Lett. **101**, 015301 (2008)
35. D. Kivotides, C.F. Barenghi, Y.A. Sergeev, Phys. Rev. B **77**, 014527 (2008)
36. A. Leonard, Phys. Fluids **6**, 765 (1994)
37. G.S. Winckelmans, A. Leonard, J. Comput. Phys. **2**, 247 (1993)
38. R.P. Feynman, Prog. Low Temp. Phys. **I**, 16 (1957)
39. K.W. Schwarz, Phys. Rev. B **31**, 5782 (1985)
40. D. Kivotides, A. Leonard, EPL **63**, 354 (2003)
41. G.E. Volovik, JETP Lett. **78**, 533 (2003)
42. A. Leonard, Ann. Rev. Fluid Mech. **17**, 523 (1985)
43. A. Leonard, J. Comput. Phys. **37**, 289 (1980)

44. J.C.R. Hunt, J.C. Vassilicos (eds.), *Turbulence Structure and Vortex Dynamics* (Cambridge University Press, Cambridge, 2001)
45. P.-E. Roche, P. Diribarne, T. Didelot, O. Francais, L. Rousseau, H. Willaime, EPL **77**, 66002 (2007)
46. P.-E. Roche, C.F. Barenghi, EPL **81**, 36002 (2008)
47. A.P. Bassom, A.D. Gilbert, J. Fluid Mech. **371**, 109 (1998)
48. D.I. Pullin, T.S. Lundgren, Phys. Fluids **13**, 2553 (2001)
49. A.P. Bassom, A.D. Gilbert, J. Fluid Mech. **398**, 245 (1999)
50. D. Kivotides, C.F. Barenghi, D.C. Samuels, Phys. Rev. Lett. **87**, 155301 (2001)
51. D. Kivotides, J.C. Vassilicos, D.C. Samuels, C.F. Barenghi, EPL **57**, 845 (2002)
52. D. Kivotides, J.C. Vassilicos, C.F. Barenghi, M.A.I. Khan, D.C. Samuels, Phys. Rev. Lett. **87**, 275302 (2001)
53. D. Kivotides, Phys. Lett. A **326**, 423 (2004)
54. O.C. Idowu, A. Willis, C.F. Barenghi, D.C. Samuels, Phys. Rev. B **62**, 3409 (2000)
55. D. Kivotides, C.F. Barenghi, D.C. Samuels, EPL **54**, 774 (2001)
56. D. Kivotides, Phys. Lett. A **341**, 193 (2005)
57. M.S. Paoletti, M.E. Fisher, K.R. Sreenivasan, D.P. Lathrop, Phys. Rev. Lett. **101**, 154501 (2008)
58. D. Kivotides, S.L. Wilkin, J. Fluid Mech. **605**, 367 (2008)